The EMBO Journal vol.4 no.11 pp.2781–2792, 1985

Apical and basolateral endocytosis in Madin-Darby canine kidney (MDCK) cells grown on nitrocellulose filters

Carl-Henrik von Bonsdorff[1], Stephen D.Fuller and Kai Simons

European Molecular Biology Laboratory, Postfach 10.2209, D-6900 Heidelberg, FRG

[1]Present address: Department of Virology, University of Helsinki, Haartmaninkatu 3, SF-00290 Helsinki, Finland

Communicated by K.Simons

Madin-Darby canine kidney (MDCK) cells (strain I) grown on 0.45 μm pore size nitrocellulose filters formed monolayers which were highly polarized and had high transepithelial electrical resistance (>3000 ohm × cm²). Morphometric analysis showed that the area of the basolateral surface domain was 7.6 times larger than that of the apical. The uptake of fluid-phase markers [³H]inulin and horseradish peroxidase (HRP) was studied from the apical and the basal side of the monolayer. Uptake of [³H]inulin was biphasic and the rate during the first 40 min corresponded to a fluid phase uptake of 20.5×10^{-8} nl/min per cell from the basolateral side, and 1.0×10^{-8} nl/min per cell from the apical side. Electron micrographs of the monolayers after HRP uptake showed that the marker was rapidly delivered into endosome-like vesicles and into multivesicular bodies. No labelling of the Golgi complex could be observed during 2 h of uptake. Evidence was obtained for the transport of fluid phase markers across the cell. HRP and fluorescein isothiocyanate-dextran crossed the monolayers in either direction at a rate corresponding to ~ 3×10^{-8} nl of fluid/min/cell. Adding the transcytosis rate to the rate of fluid accumulation into the cell yielded a total basolateral endocytic rate which was 6-fold greater than the apical rate. When the uptake rates were normalized for membrane area the apical and basolateral endocytic rates were about equal per unit cell surface area.

Key words: cell polarity/epithelial cells/fluid phase uptake/morphometry/transcytosis

Introduction

The plasma membrane of cells in an epithelium is separated by junctional complexes into the apical and the basolateral domains (for reviews, see Rodriguez-Boulan, 1983; Simons and Fuller, 1985). These two domains of the epithelial cell surface have different protein and lipid compositions. Membrane is continuously endocytosed from both the apical and basolateral domains which are replenished by membrane recycling (see Steinman *et al.*, 1983). Since most studies on endocytosis in epithelial cells have been carried out on whole tissue (Oliver and Hand, 1978; Abrahamson and Rodewald, 1981; Oliver, 1982; Christensen, 1982; Herzog, 1983, 1984; Gonnella and Neutra, 1984; Wall and Maack, 1985) access has been limited to one side of the epithelium. Little is known of the quantitative aspects of the apical and basolateral endocytosis in any epithelial cell.

We have grown Madin-Darby canine kidney (MDCK) cells on nitrocellulose fitlers. The MDCK strain I cells (Richardson *et al.*, 1981; Valentich, 1981; Balcarova-Ständer *et al.*, 1984) form monolayers with very high transepithelial resistances (>3000 ohm × cm²) (Fuller *et al.*, 1984). The cells in the monolayer express all the characteristic features of polarized epithelial cells seen *in vivo* (Simons and Fuller, 1985). Using this experimental system it was possible to determine separately the uptake of fluid phase markers from both the apical and the basolateral sides of the MDCK-cell monolayers, and to measure the transcytosis rate in each direction. The rates measured could then be correlated with the surface areas of the two domains which were determined by morphometric analysis. These estimates yielded the first quantitative view of the endocytosis and transcytosis in a polarized epithelial cell layer.

Results

Characterization of the filter-grown MDCK monolayers

The clone 8-1B of the low-passage strain I MDCK cells used in our laboratory was selected for its ability to form tight monolayers on large pore size (3.0 μm) nitrocellulose filters (Fuller *et al.*, 1984). Fully polarized monolayers are obtained after 3–4 days of growth (Balcarova-Ständer *et al.*, 1984). The cells were grown on 0.45 μm filters because the electrical resistance of the monolayer was somewhat more stable than on the larger pore size filters (Fuller *et al.*, 1984). Under these conditions the monolayers contained $2.9 \pm 0.4 \times 10^6$ cells per filter in an area of 3.14 cm² after 4 days of growth.

The cells forming the monolayer are roughly cuboidal (Figure 1A). A typical cell (Figure 1B) has a basally located nucleus with a deeply folded nuclear envelope and is surrounded by glycogen deposits as seen in this tannic acid contrasted micrograph. Our standard processing procedure leaves glycogen deposits (Gly) unstained. The Golgi complex is supra-nuclear as Figure 2B, a tangential section through one cell at the level of the Golgi complex, shows. The lateral membranes of the neighbouring cells run closely apposed to each other forming interdigitating folds and are connected by numerous desmosomes (Figure 2B). Along the lateral membrane small (50–100 nm diameter) vesicle profiles are seen pinching off or fusing with the plasma membrane (Figure 2B). Many of these vesicle profiles are open to the extracellular space since they are stained by horseradish peroxidase (HRP) (see later). Numerous short microvilli are present on the apical surface and many vesicles (100–300 nm) are found in the cytoplasm just under the membrane. Some of these had amorphous electron-dense contents (Figure 2A).

Morphometric analysis was performed as described in the Appendix to determine the surface areas of the apical and the basolateral membrane of the cell. The main features of both MDCK strain I and II cells grown on filters are given in Table I of the Appendix. In the strain I cells less than one seventh of the total plasma membrane surface area is apical.

Uptake of fluid-phase markers

Fluid phase uptake of the strain I MDCK cells was studied with the cells grown on 0.45 μm nitrocellulose filters in mini-Mar-

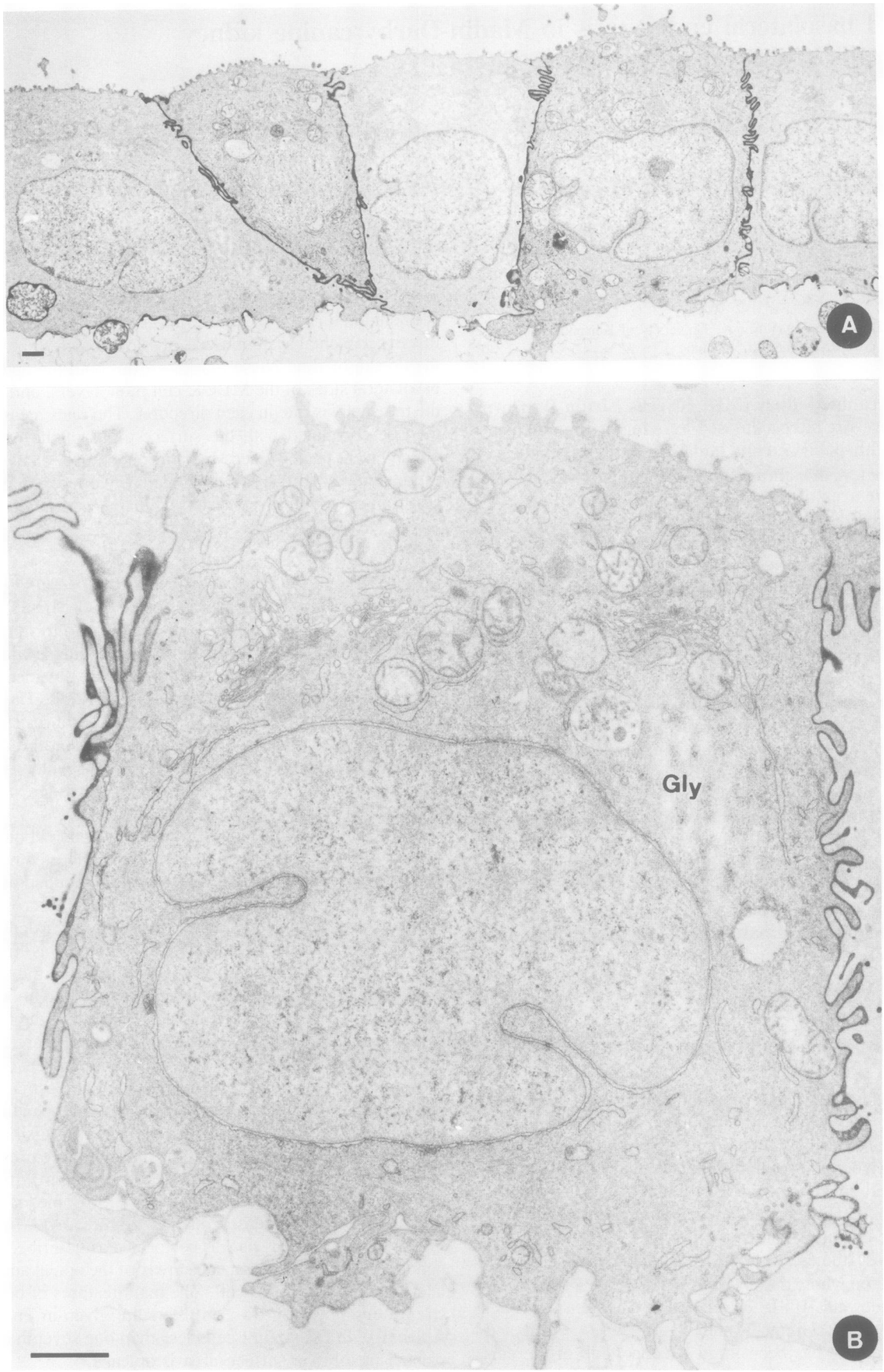

Fig. 1. Electron micrographs of the monolayer of strain I MDCK cells on a nitrocellulose filter. The cells have been sectioned perpendicular to the filter. Tannic acid staining has been used to visualize the lateral boundaries between the cells. **(A)** Low-power micrograph showing the typical cuboidal appearance of the monolayer with basal location of the nuclei. The basal aspect of the cell does not penetrate deeply into the filter which is at the bottom of the figure. Bar: 5 μm. **(B)** A single cell showing typical polar features of the strain I MDCK cell. Poorly stained glycogen deposits are indicated by Gly. Bar: 1 μm.

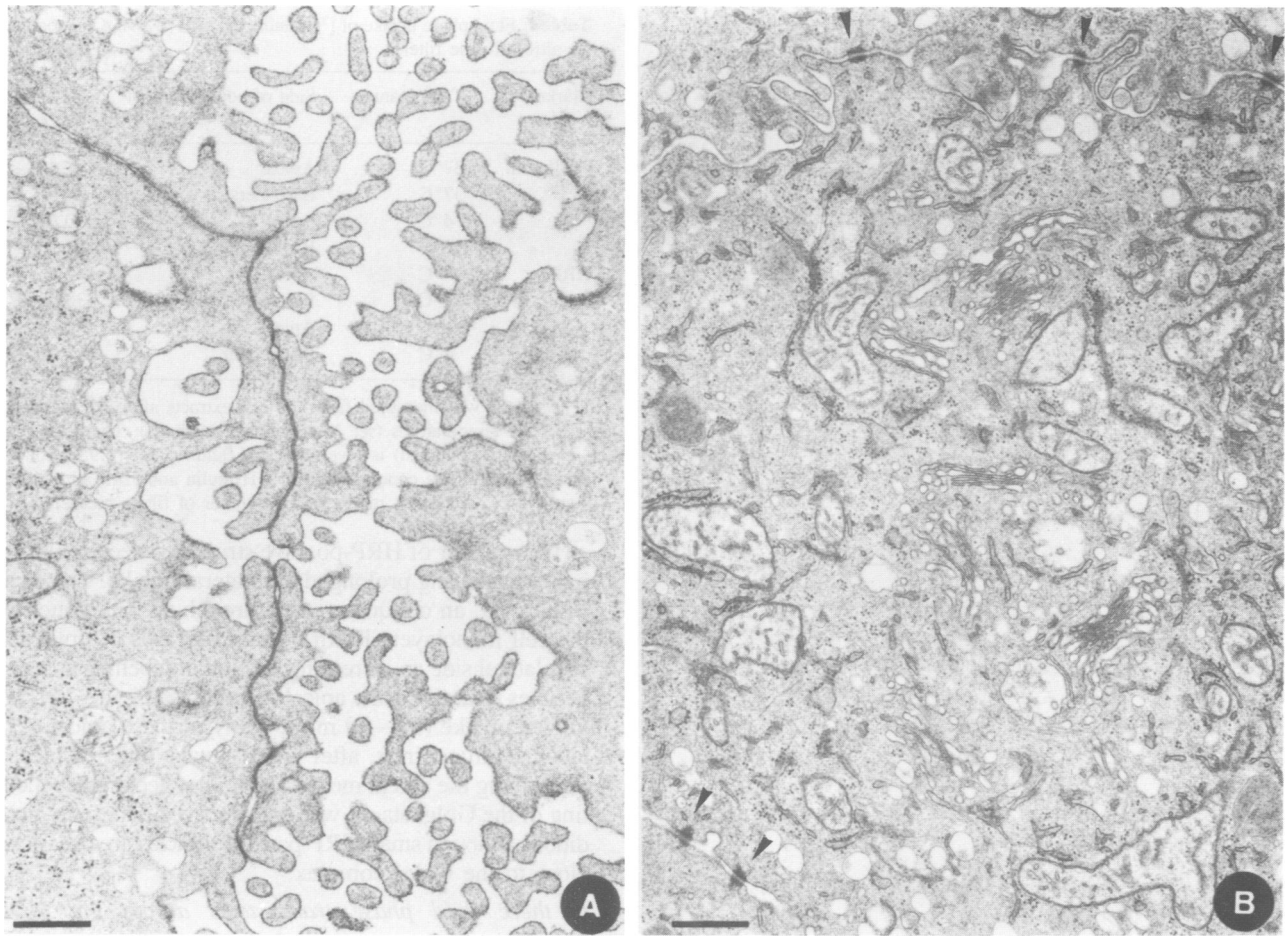

Fig. 2. Electron micrographs of the MDCK cells sectioned parallel to the monolayer. **(A)** A section of the most apical part of the cells showing cross-cut microvilli and the layer of vesicles just under the apical membrane. The section passes through the tight junctional region of the cells. Bar: 0.5 μm. **(B)** A section cut at the supranuclear level shows the presence of numerous Golgi cisternae (compare Figure 1B). Desmosomes are marked with arrowheads. Bar: 0.5 μm.

brook chambers so that uptake from each side could be measured separately. Figure 3 shows the uptake of [^{3}H]inulin over a period of 2 h at 37°C from the apical (Figure 3A) and the basolateral (Figure 3B) sides. The background due to binding of the marker to the monolayers (and filter) was determined by parallel incubations at 4°C and this value was subtracted from the values determined at 37°C. The cell-associated radioactivity was converted to fluid phase volume using the specific activity of the original medium. These corrected uptake values showed that the rate of fluid accumulation was biphasic (Figure 3C). An uptake of $20.5 \pm 2.1 \times 10^{-8}$ nl/cell/min was calculated from the rate observed during the first 40 min of uptake from the basolateral side. Thereafter, uptake slowed to a rate of 5.1×10^{-8} nl/cell/min. In contrast, the net apical uptake was found to be only $1.0 \pm 0.1 \times 10^{-8}$ nl/cell/min during the first 40 min of uptake (Figure 3C). Thus, the apical rate is ~20 times less than the basolateral.

When HRP was used as a marker for fluid phase endocytosis the value measured after 1 h of uptake was similar to that observed with [^{3}H]inulin (Table I). The apical uptake of HRP was low, the net uptake being 1.0 nl/h/filter. The basolateral uptake for inulin and for HRP was 27.2 and 30.2 nl/h/filter, respectively.

Visualization of HRP uptake

The location of the HRP internalized by the cells was visualized by electron microscopy after polar administration for time periods from 1 min and 2 h. HRP was used in concentrations varying from 0.5 to 10 mg/ml diluted in Eagle's minimum essential medium with Earle's salts (E-MEM). Figure 4 shows electron micrographs of thin sections of MDCK cells after 3 min exposure to HRP. The monolayers were fixed without previous wash. This procedure leaves the plasma membrane stained with HRP reaction product. If washed before fixing, the plasma membrane was free of HRP (results not shown). Apically administered HRP is found in small (100–200 nm) and in larger (300–500 nm) endosome-like vesicles (Figure 4A). Basolaterally administered HRP labels similar structures (Figure 4B), located mainly near the lateral membrane and more rarely near the basal membrane (Figure 7A). Many of the profiles seen along the lateral membranes are not closed vesicles. Serial sections of cells labelled with HRP after glutaraldehyde fixation show that most of these structures are open to the lateral extracellular space (data not shown). HRP-labelled coated pits and vesicles can be observed close to the membranes (Figure 5).

The overall distribution of HRP-positive vesicles remained the same (Figure 6) even after prolonged uptake from the apical side; 90% of the HRP-labelled vesicles is in the apical one-third of the cells. HRP-positive vesicles are rare in the basal part of the cell. The section in Figure 6 shows more HRP-positive vesicles than average.

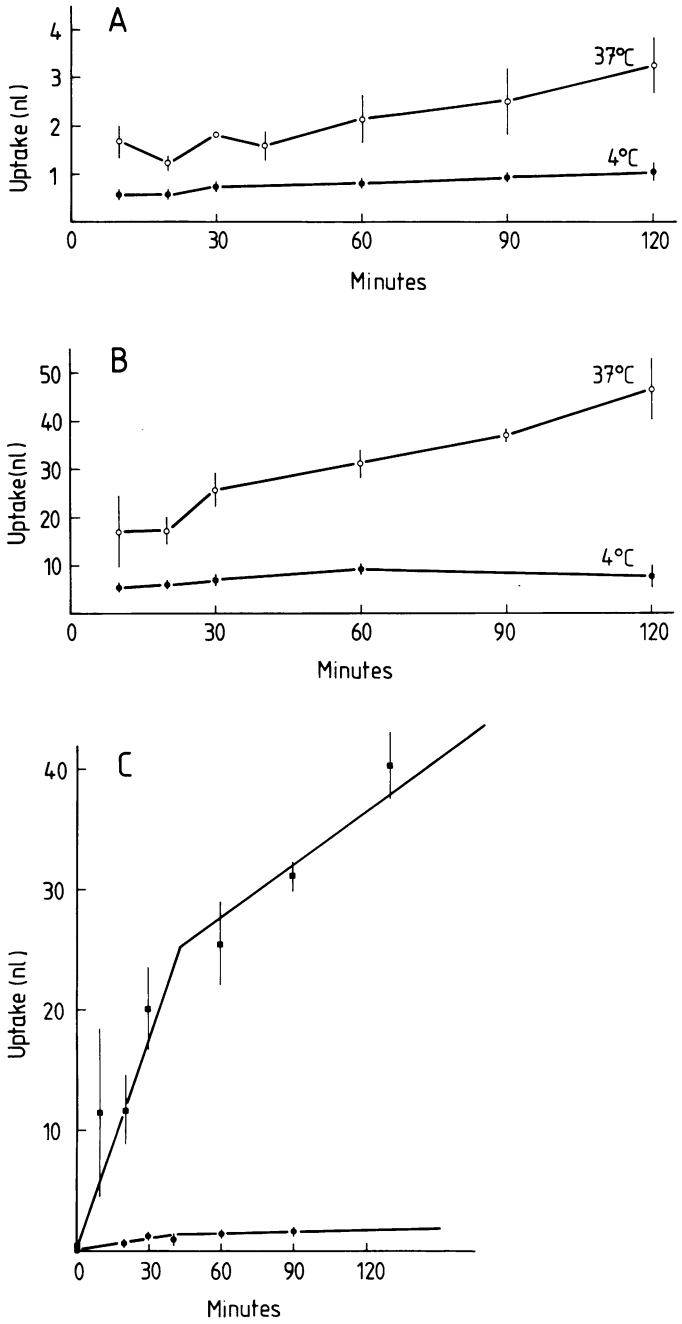

Fig. 3. Polar uptake of the fluid phase marker inulin by MDCK cells. The ^{3}H-labelled marker was administered in the apical or basolateral medium of the cells grown on filters. **Panel A:** total uptake from the apical side. **Panel B:** total uptake from the basolateral side. After the desired incubation period at 37°C (○—○) or 4°C (●—●), the monolayers were washed at 0°C and extracted. The radioactivity in the extract was then converted into the corresponding volume of fluid using the concentration of [^{3}H]inulin in the medium at the start of the uptake. Each point in the graph represents the mean of three filters and the bar shows the standard error of the mean. **Panel C:** this graph shows the background-corrected values for the uptake from the apical (●—●) and basolateral (■—■) sides. Separate weighted least squares regression lines are drawn through the time points before and after 40 min. The vertical bar shows the standard deviations. The time points prior to 40 min were fitted to a least squares regression line, constrained to pass through the origin. An analysis of variance showed that the points corresponding to later times did not fall on this line and hence were fitted by separate least squares regression. The slopes of these lines are 20.5 $\pm$2.1 $\times$ 10^{-8} nl/cell/min (before 40 min) and 5.1 $\times$ 10^{-8} nl/cell/min (after 40 min) for the basolateral uptake. The apical uptake during the first 40 min occurred with a rate of 1.0 $\pm$ 0.1 $\times$ 10^{-8} nl/cell/min.

Table I. Fluid phase uptake of [^{3}H]inulin and HRP by MDCK monolayers grown on nitrocellulose filters

Marker	Temperature	Side of administration	Uptake[a] (nl per h)
[^{3}H]Inulin	37°C	Apical	1.45 ± 0.6 (6)
	37°C	Basolateral	34.8 ± 4.9 (9)
	4°C	Apical	0.6 ± 0.3 (5)
	4°C	Basolateral	7.5 ± 2.3 (8)
HRP	37°C	Apical	1.0 ± 0.01 (6)
	37°C	Basolateral	38.9 ± 7.5 (8)
	4°C	Apical	<0.3 (4)
	4°C	Basolateral	8.7 ± 3.5 (6)

[a]The uptake was measured from the cell extracts after 1 h incubation at respective temperatures (see Materials and methods). The uptake (± standard deviation) is given as nl of fluid/h/filter (2.9 $\times$ 10^6 cells), calculated from the concentration of [^{3}H]inulin and HRP administered. The numbers in parenthesis represent the number of filters measured.

The number of HRP-positive structures deeper within the cell increases during prolonged basolateral uptake. This is shown in Figure 7B, an oblique section through the supranuclear part of the cell monolayer. From 30 min onwards of uptake from the basolateral side an increasing amount of labelling is seen in small vesicles underlying the apical membrane (Figure 7C). After prolonged uptake (60 – 80 min), many of these apical vesicles are labelled. In contrast, after apical uptake of HRP these vesicles underlying the apical membrane do not become labelled. Labelling of the Golgi stacks was not observed under any uptake conditions although small HRP-positive vesicles are occasionally seen close to the Golgi complex.

Is there fluid phase transcytosis across the MDCK cell monolayer?

The morphological studies of HRP uptake from the basolateral side suggest a transcytic route through the cell. We quantitated the extent of this traffic using the transport device shown in Figure 8. Table II summarizes the transcytosis values obtained for HRP and fluorescein isothiocyanate (FITC)-dextran at 37°C. The rate for HRP crossing the monolayer at 4°C was used as an estimate of the contribution of leakage to the transcytosis rate. This value was subtracted from the total rate to yield the transcytosis rate. Approximately 3 $\times$ 10^{-8} nl of fluid is passed across the cell per min in each direction.

Discussion

This work presents measurements of internalization and transcytosis of fluid phase markers from both the apical and the basolateral sides of an epithelium; namely MDCK strain I cells grown on nitrocellulose filters. These cells form very tight epithelial monolayers with high transepithelial resistances (Richardson *et al.*, 1981; Fuller *et al.*, 1984; Balcarova-Ständer *et al.*, 1984). The tightness of the monolayer was evaluated at the end of each experiment by determining the electrical resistance across the filter. This is a useful test in studies of this type where errors due to paracellular leaks are a constant problem. The rate of label internalization from the apical and the basolateral sides was biphasic. The rate of endocytosis from the apical side was only 1.0 $\pm$ 0.1 $\times$ 10^{-8} nl of fluid internalized per cell per min during the first 40 min of uptake, whereas the corresponding fluid uptake from the basolateral side was 20-fold greater (20.5 $\pm$ 2.1 $\times$ 10^{-8} nl/cell/min). At later times (>40 min) lower, presumably steady-state, rates were observed with both apical and basolateral administration. We assume that the decrease of the

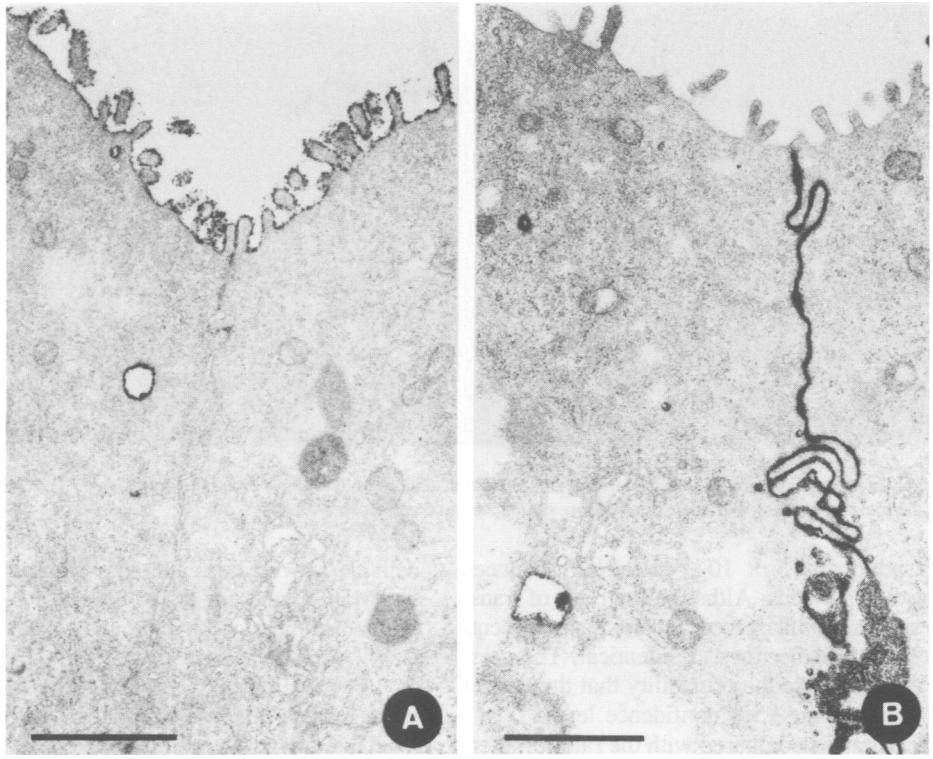

Fig. 4. Electron micrographs of MDCK cells after short-time HRP uptake from **(A)** apical and **(B)** basolateral side. HRP (10 mg/ml) had been administered for 3 min and the monolayers were then fixed without previous wash. Bar: 0.5 μm.

Fig. 5. Electron micrograph of the lateral membranes of two adjacent cells 30 min after HRP (10 mg/ml) administration from the basolateral side. Several coated vesicles (arrowheads) containing HRP stain can be seen. Bar: 0.5 μm.

rate of internalization is due to the filling of intracellular compartment(s) into which the marker accumulates.

Electron microscopic observation confirmed that considerably fewer vesicles positive for the HRP reaction were seen at all times after apical administration of the enzyme than were observed after basolateral application. Similar conclusions were obtained by following the internalization of FITC-dextran by light microscopy in MDCK-I cells grown on filters (K.Simons and C.-H.von Bonsdorff, unpublished observations). The apically applied HRP is delivered into vacuoles, apparently endosomes, multivesicular bodies and lysosomes, located mainly in the supranuclear (apical) part of the MDCK cell. These seemed to fill rapidly and there appeared to be no substantial increase in the number of HRP-positive vesicles beyond 30 min of endocytosis. HRP applied to the basolateral side appears first in vacuoles along the lateral and, to a much lesser extent, along the basal border. After 30 min of uptake endosomes, multivesicular bodies and lysosomes in the apical region also become stained. The appearance of stain in the 100 – 300 nm vesicles close to the apical membrane is particularly striking. HRP was never detected in Golgi cisternae at any stage.

Many instances of receptor-mediated transcytosis in epithelial cells have been studied (Brandzaeg, 1974; Renston *et al.*, 1980; Abrahamson and Rodewald, 1981; van Deurs *et al.*, 1981; Herzog, 1983; Geuze *et al.*, 1984). Transcytosis is probably a general property of polarized epithelia, but little is known of the magnitude of the total vesicular traffic connecting the apical and the transcytosis surfaces. We quantitated the passage of fluid-phase markers across the filter-grown MDCK cells. The precision of our transcytosis rates was not as high as that of our internalization rates. This reflects the fact that the transcytosis measurements are much more tedious and limited in number by leakage induced by manipulation. The rates for the transcytosis measured with two markers (HRP, 40 kd and FITC-dextran-70, 70 kd) in

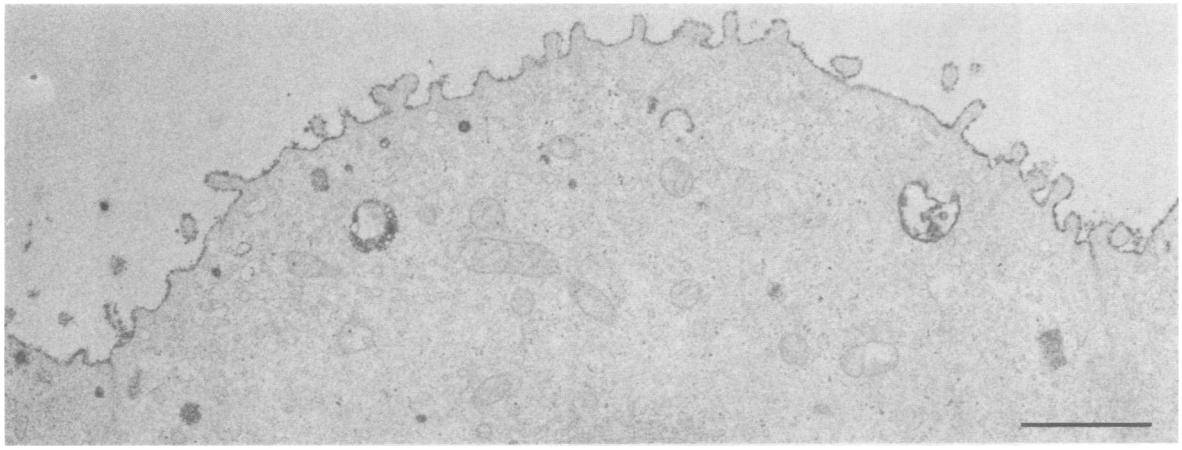

Fig. 6. Electron micrograph of the apical part of a cell after 1 h administration of HRP (10 mg/ml) from the apical side. This section contains more HRP-positive vesicles than in the average section, but their distribution and appearance are typical. Bar: 0.5 μm.

MDCK I cells corresponded to 3×10^{-8} nl/cell/min between the apical and the basolateral sides. Although the rates of transcytosis from the two sides are similar, more precise measurements would be needed to show whether they are identical. The present data only allow us to exclude the possibility that they differ by a factor of 2 or more at the 95% confidence level.

When the transcytosis rate is compared with the rates of internalization measured from the early phase of marker uptake (Figure 3C), it represents only a fraction of the basolateral internalization rate. In contrast, the rate of internalization from the apical side is lower than the measured transcytosis rate. This reflects the fact that the compartments into which the fluid phase markers accumulate inside the cell seem to be small and are rapidly filled as shown by both the microscopy and the measured internalization rate. Therefore, it was difficult to measure the true initial rate of endocytosis from the apical side, i.e., before transcytosis has started to deplete the intracellular pool of internalized marker. Moreover, our determination of the internalization rate does not include the possible short-circuiting of fluid-phase markers returned to the apical side during membrane recycling (Besterman *et al.*, 1981; Steinman *et al.*, 1983), but this should amount to only a fraction of the total uptake. Without these values we cannot obtain an exact measure of the total rate of apical endocytosis. However, a reasonable approximation to the total endocytic rate should be obtained by combining the measured rate of internalization with the transcytosis rate. This gives an upper limit for the total rate (discounting short-circuiting). Total fluid uptake was thus $\sim 4 \times 10^{-8}$ nl/cell/min from the apical side compared with 23.5×10^{-8} nl/cell/min from the basolateral side.

The ratio of basolateral to apical fluid uptake is 5.7. Morphometry was done so that this value could be expressed in terms of the surface areas of the two plasma membrane domains. Our morphometric measurements showed that the surface area of the apical membrane of the average MDCK I cell is $\sim 1/7$th of that of the basolateral membrane. Therefore, the uptake rates normalized for membrane area are very similar for the apical and the basolateral sides, 0.019×10^{-8} versus 0.015×10^{-8} nl/min/μm^2, respectively. Comparisons with a non-polarized cell such as the BHK cell which has an average surface area of 3400 μm^2 (Griffiths *et al.*, 1984) and a fluid phase uptake rate of 62×10^{-8} nl/cell/min (Marsh and Helenius, 1980) giving a rate of 0.018×10^{-8} nl/min/μm^2, demonstrates that fluid internalization proceeds with similar rates per unit surface area in these cells. However, this cannot be generalized. The endocytic rates for MDCK and for BHK cells are clearly slower than those previously measured by Steinman *et al.* (1976) for macrophages, 0.14×10^{-8} nl/min/μm^2, and L cells, 0.038×10^{-8} nl/min/μm^2. None of these estimates for the endocytic rates include the possible short-circuiting of the fluid phase markers during membrane recycling.

The measured fluid uptake in BHK cells corresponds to 2300 coated vesicles of 90 nm diameter per cell per min (Marsh and Helenius, 1980). Assuming that vesicles of similar size carry the estimated 3×10^{-8} nl of fluid across the MDCK I cells, 100 such vesicles would traverse the cell per min in each direction. Thus, there is a substantial amount of membrane traffic connecting the two surface domains. These rates imply that sorting of internalized membrane components has to occur at some stage of the transcellular route to prevent intermixing of the apical and the basolateral membrane domains. The exact route of the transcellular traffic is not yet known. We have recently shown that the vesicular stomatitis virus G protein implanted into the apical domain is passed across the cell to the basolateral membrane. The G protein (Matlin *et al.*, 1983; Pesonen and Simons, 1983) is internalized from the apical membrane into endosomes, and from there passed to the basolateral membrane (Pesonen *et al.*, 1984a). No evidence was found for involvement of lysosomes and Golgi complex in the transcellular route (Pesonen *et al.*, 1984b). Previous morphological studies of the route of receptor-mediated transcytosis in other epithelial cells have led to similar conclusions (Abrahamson and Rodewald, 1981; Herzog, 1983; Geuze *et al.*, 1984). However, the available evidence does not exclude the possibility that the transcytic pathway shares compartments with the exocytic. More careful mapping of those pathways is needed to address this question and to identify the sites of sorting.

Materials and methods

Cells

All transport studies were carried out with strain I MDCK cells (Richardson *et al.*, 1981). The cells were seeded on 0.45 μm pore size nitrocellulose filters (HATF 02500, Millipore France S.A., Molsheim, France) in mini-Marbrook chambers (MMC) with an inner diameter of 20 mm, as described (Fuller *et al.*, 1984) and used between 4 and 6 days after seeding.

The monolayers were screened for their electrical resistance as described by Fuller *et al.* (1984). All monolayers used had an electrical resistance >3000 ohm $\times$ cm^2.

The strain II MDCK cells have been described by Louvard (1980) and they

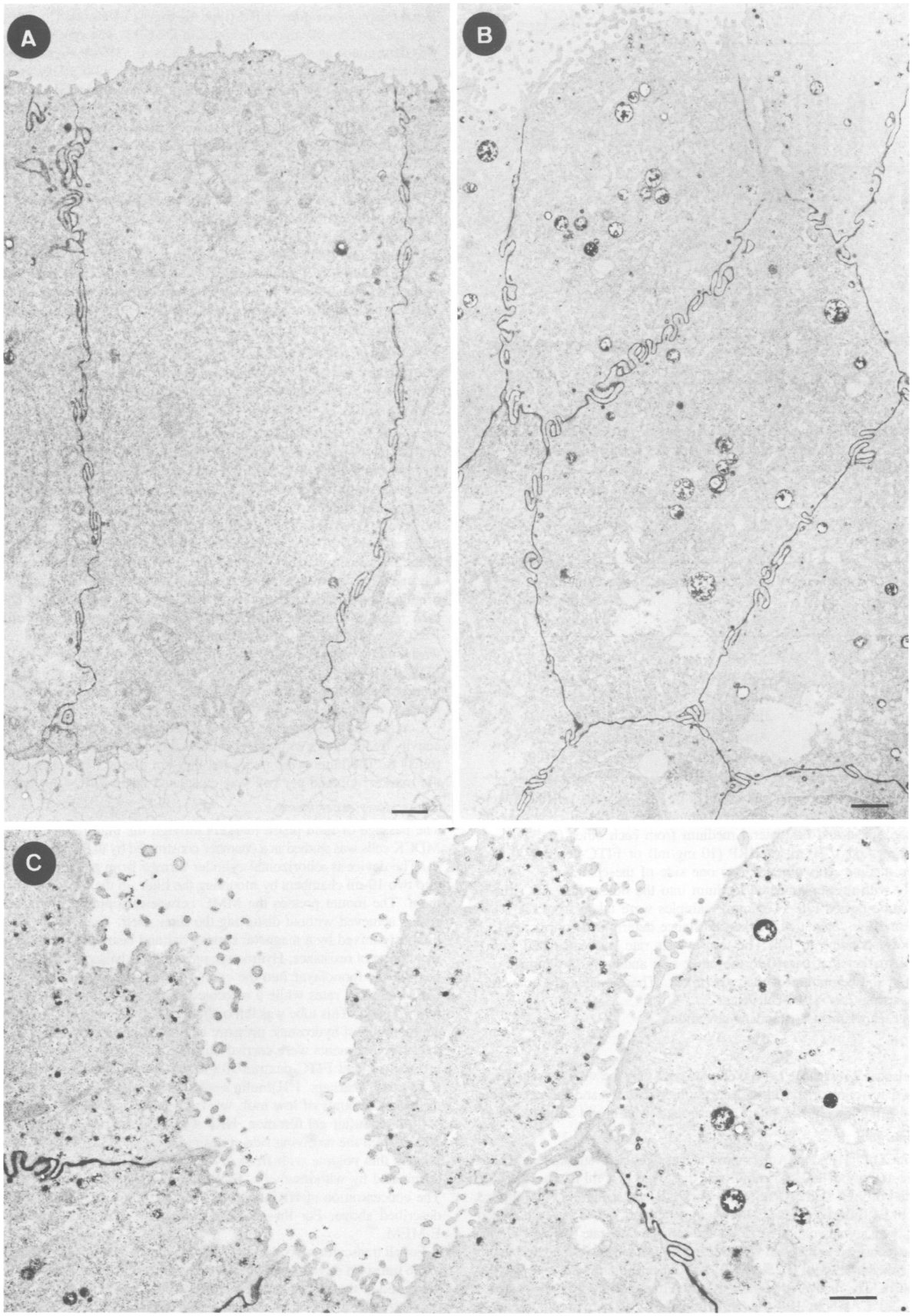

Fig. 7. Electron micrographs of HRP uptake from the basolateral side. **(A)** Cross-section through a cell after 30 min of HRP uptake (10 mg/ml). Most of the label is seen in small (< 300 nm) vesicles which are distributed along the lateral membrane but also to some extent at the apical membrane. Bar: 1 μm. **(B)** An oblique section through the monolayer extending from the microvilli at the upper left to the nuclear region at the bottom after 80 min exposure to HRP. Numerous multivesicular bodies can be seen. Bar: 1 μm. **(C)** The enrichment of HRP-positive vesicles underneath the apical membrane is shown in this section cut almost parallel to the monolayer. HRP incubation for 60 min. Bar: 0.5 μm.

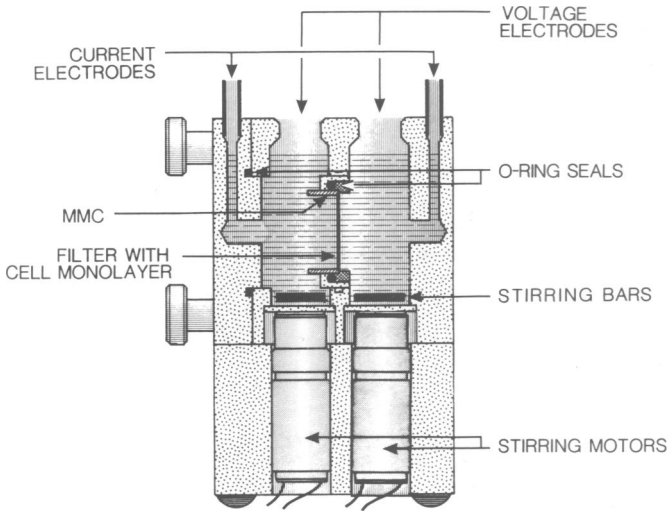

Fig. 8. A cross-section of the device used to measure transcytosis. The cell monolayer in a filter mounted in a mini-Marbrook chamber is located between two 10-ml chambers (see Materials and methods).

Table II. Transcytosis of fluid phase markers by MDCK monolayers on nitrocellulose filters

Marker[a]	Temperature	Side of administration	Volume passed across the filter[b] (nl per h)
HRP	37°C	Apical	8.4 ± 2.6
	37°C	Basolateral	7.8 ± 3.0
	4°C	Apical	2.6 ± 0.5
	4°C	Basolateral	3.8 ± 0.1
FITC-dextran	37°C	Apical	7.8 ± 2.3
	37°C	Basolateral	8.7 ± 0.9

[a]For these experiments 4–6-day-old cultures of MDCK cells on filters were used. The mini-Marbrook chambers were mounted in a special chamber which seals the apical and basolateral medium from each other (see Materials and methods). 10 ml of HRP (10 mg/ml) or FITC-dextran-70 (10 mg/ml) in medium was pipetted into one side of the chamber simultaneously with unsupplemented medium into the other side. After the desired incubation period (30–120 min), samples were taken from the receiver side and the content of marker substance determined, normalized to the amount corresponding to 1 h. The transcytosis rate was calculated from the amount of marker that passed to the other side and from the known concentration at the beginning of the experiment. These values are converted to nl/cell/min using 2.9×10^6 cells/filter.
[b]Mean of three experiments ± standard deviation.

have a lower electrical resistance (~ 100 ohm × cm²) than the strain I cells. These cells were used for comparison in the morphometric study and the cells were grown on 0.45 μm nitrocellulose filters as described (Matlin and Simons, 1984).

Fluid phase markers

[³H]inulin. 1 mCi of [³H]inulin (Amersham Buchler GmbH, Braunschweig, FRG) with a specific activity of 1.03 Ci/mmol was dissolved in 1 ml of Ca- and Mg-free phosphate-buffered saline [PBS(−)]. The radioactive marker was applied to a 50 × 1 cm P4 Biogel column (Calbiochem, Frankfurt, FRG) pre-equilibrated with E-MEM, with a void volume of 15 ml and run at a flow-rate of 0.25 ml/min. [³H]Inulin was recovered in the void volume, and supplemented with bovine serum albumin to a concentration of 0.2% (w/v). This material had a specific activity of ~50 c.p.m./nl. The recovered marker was used immediately for uptake studies or stored at −20°C. About 10% of the original radioactivity was completely included into Biogel P4 matrix and might represent $[^3H]_2O$.

The radioactivity of the extracts was determined by counting a 500 μl aliquot of the extraction solution (see below) in 10 ml of Rotiszint-22 fluid (Carl Roth, Karlsruhe, FRG) in a liquid scintillation counter. Dilutions of the input markers were made in the same extraction solutions and counted from the same volumes.

Horseradish peroxidase. HRP (type II, Sigma Chemical Co., St. Louis, MO) was used at 0.5–10 mg/ml dissolved in E-MEM. The concentration of the tracer was determined as described by Steinman *et al.* (1976). Fresh substrate solution was prepared for each experiment and contained 1 ml 0.3% (v/v) H_2O_2, 0.82 ml of 1.33% (w/v) O-dianisidine-di-hydrochloride in water added to 100 ml of 0.05 M phosphate buffer, pH 5.0. The sample (10–100 μl) was added to 1 ml of the substrate solution, mixed carefully and 200 μl was transferred to a well of a microtiter plate (Nunc, Kamstrup, Denmark). The development of colour was measured at 30-sec intervals in a Uniscan photometer (Labsystems, Helsinki, Finland) at 495 nm.

The inactivation of HRP in the MDCK cells was determined by incubating the cells with HRP (10 mg/ml) from the basolateral side for 1 h. The monolayers were then washed at 4°C as described below, filters removed from the chambers and placed into individual 3-cm diameter Petri dishes in 1 ml medium and incubated for up to 6 h. Triplicate filters were taken as samples each hour. The HRP content was determined in the medium and in the cell extracts. It was found that HRP was inactivated at a linear rate of 5%/h presumably due to lysosomal degradation (data not shown).

FITC-dextran. FITC-dextran-70 (70 kd, Sigma) was assayed by measuring the fluorescence intensity with an excitation wavelength of 490 nm and an emission wavelength of 520 nm in a Perkins/Elmer fluorospectrophotometer (Pesonen and Simons, 1983).

Uptake of fluid phase markers. First, the electrical resistance of the cell monolayers in MMCs was monitored to be sure that the monolayer was tight, then the monolayer was rinsed briefly in E-MEM supplemented with 0.2% bovine serum albumin and placed into individual (10 ml) cups, cells up (for apical uptake) or filter up (for basolateral uptake). The level of the medium outside the MMC just exceeded the level of the filter. The medium over the filter was carefully aspirated and replaced with 300 μl of the same medium containing the desired concentration of the fluid phase marker ([³H]inulin or HRP). After incubation for various times, the marker solution was removed and the filter was brought rapidly to 0°C by briefly dipping it in three successive washes of ice-cold PBS(−). The filters were then removed from the MMCs and washed five times for 10 min in 5 ml of PBS(−) with shaking. After washing, the filters were blotted to remove excess wash solution and extracted with 1.5 ml 1% (w/v) Triton X-100, 0.5% (w/v) SDS in PBS(−) for 30 min at 4°C. In uptake experiments using [³H]inulin as marker the wash and extraction solutions contained an excess (0.1 mg/ml) of unlabelled inulin.

Controls for the uptake studies comprised 'uptake' at 4°C and 'uptake' of radioactivity by the filters without cells that had been pre-incubated in growth medium for 24 h. The latter were incubated in 3-cm plastic Petri dishes with 300 μl of the marker. Uptake per cell was calculated using 2.9×10^6 cells/filter.

Transcytosis experiments

The passage of fluid phase markers through the high-resistance monolayers of MDCK cells was studied in a chamber constructed by the EMBL workshop (Figure 8). The device is a horizontal cylinder formed from plexiglass which is divided into two 10-ml chambers by mounting the filter, in the MMC, vertically between them. The mount presses the MMC between neoprene gaskets so that a tight seal is achieved without distorting the filter itself. Each 10-ml chamber is continuously mixed by a magnetic stirring bar and bears ports for sampling and the monitoring of resistance. Hydrostatic pressure was balanced by clamping the MMC bearing the monolayer into the empty device and filling the chambers with E-MEM at equal rates while a separate, air-filled tube between the chambers remained open. This tube was left open during movement of the chamber to allow equilibration of hydrostatic pressure but closed during experiments with a Teflon valve. Experiments were carried out in a 37°C room or in a 4°C room. HRP (10 mg/ml) and FITC-dextran-70 (10 mg/ml) diluted in E-MEM were used as fluid phase markers. [³H]Inulin could not be used for this purpose because of the small amounts of low mol. wt. (and hence rapidly diffusing) contaminants still present after gel filtration. HRP was monitored by withdrawing samples of 200 μl from the receiving side at desired time intervals (usually 30 min) and replacing this volume with fresh E-MEM. The FITC-dextran experiments were terminated by withdrawing a 3-ml sample at the end of the incubation period. The concentration of HRP and of FITC-dextran in the medium was assayed as described above. For these determinations the standards were also diluted in E-MEM.

For all transcytosis experiments, monolayers in MMCs were transferred directly to the transport device without measuring the electrical resistance. Resistance was measured at the end of the experiment in the transport device. This procedure minimized handling of the monolayers. Despite this precaution only 20% of the filters showed no leakage at the end of the experiment. These filters were found to have a resistance of >2000 ohm × cm².

The binding of HRP to the filter was determined by allowing minute concentrations (25–100 ng/ml) of HRP to diffuse through filters mounted in the MMC. The filters were devoid of cells and had been incubated for 24 h in the growth

medium prior to the experiment. A linear rate was observed with these HRP concentrations (data not shown). Since these levels are much lower than those used in our work we conclude that binding of HRP to the filter did not affect our transcytosis or uptake results.

Cell counts

The number of cells on the filters was determined as described by Fuller *et al.* (1984) by counting nuclei stained with Hoechst dye 33258 (Serva, Heidelburg, FRG) from micrographs taken at 109 × magnification.

Electron microscopy

Monolayers were fixed with 0.5% glutaraldehyde in 0.1 M cacodylate buffer (pH 7.4) at room temperature for 20 min. Post-fixation was with 1% OsO_4 in cacodylate for 1 h at room temperature, followed by a cacodylate rinse and aqueous uranyl acetate (2%) *en bloc* staining for 1 h. In some instances the staining was with 1% tannic acid in cacodylate. Pieces of the filters were dehydrated, incubated in propyleneoxide for only 5 min since the monolayers tended to curl during this procedure, and were then embedded in Epon 812.

Thin sections were cut perpendicular or parallel to the monolayers with a Reichert OmU3 ultramicrotome and post-stained with uranyl acetate and lead citrate (Reynolds, 1963). Electron micrographs were taken with a Phillips 301 or 400T electron microscope. The peroxidase-containing samples were processed essentially according to Graham and Karnovsky (1966) and as described by Matlin *et al.* (1983).

Acknowledgements

The authors thank Hilkka Virta for excellent technical assistance, Mette Ohlsen for expert sectioning and electron microscopy, Annie Steiner, Joyce de Bruyn and Marianne Remy for their careful typing of a complex manuscript and Kathryn Howell, Graham Warren and Jean Davoust for critical readings of the manuscript. We thank Luis Cruz-Orive and Gareth Griffiths for advice concerning the morphometry. C.-H.von Bonsdorff was the recipient of a long-term EMBO fellowship and S.D.Fuller of a Helen Hay Whitney fellowship.

References

Abrahamson,D.R. and Rodewald,R. (1981) *J. Cell Biol.*, **91**, 270-280.
Balcarova-Ständer,J., Pfeiffer,S.E., Fuller,S.D. and Simons,K. (1984) *EMBO J.*, **3**, 2687-2694.
Besterman,J.M., Airhart,J.A., Woodworth,R.C. and Low,R.B. (1981) *J. Cell Biol.*, **91**, 716-727.
Brandtzaeg,P. (1974) *J. Immunol.*, **112**, 1553-1559.
Christensen,E.I. (1982) *Eur. J. Cell Biol.*, **29**, 43-49.
Fuller,S.D., von Bonsdorff,C.-H. and Simons,K. (1984) *Cell*, **38**, 65-77.
Geuze,H.J., Slot,J.W., Strous,G.J.A.M., Peppard,J., von Figura,K., Hasilik,A. and Schwartz,A.L. (1984) *Cell*, **37**, 195-204.
Gonnella,P.A. and Neutra,M.R. (1984) *J. Cell Biol.*, **99**, 909-917.
Graham,R.C., Jr. and Karnovsky,M.J. (1966) *J. Histochem. Cytochem.*, **14**, 291-302.
Griffiths,G., Warren,G., Quinn,P., Mathieu-Costello,D. and Hoppeler,H. (1984) *J. Cell Biol.*, **98**, 2133-2141.
Herzog,V. (1983) *J. Cell Biol.*, **97**, 607-617.
Herzog,V. (1984) *Int. Rev. Cytol.*, **91**, 107-139.
Louvard,D. (1980) *Proc. Natl. Acad. Sci. USA*, **77**, 4132-4136.
Marsh,M. and Helenius,A. (1980) *J. Mol. Biol.*, **142**, 439-454.
Matlin,K., Bainton,D.F., Pesonen,M., Louvard,D., Genty,N. and Simons,K. (1983) *J. Cell Biol.*, **97**, 627-637.
Matlin,K. and Simons,K. (1984) *J. Cell Biol.*, **99**, 2131-2139.
Oliver,M. (1982) *J. Cell Biol.*, **95**, 154-161.
Oliver,C. and Hand,A.R. (1978) *J. Cell Biol.*, **76**, 207-220.
Pesonen,M. and Simons,K. (1983) *J. Cell Biol.*, **97**, 638-643.
Pesonen,M., Ansorge,W., Simons,K. (1984a) *J. Cell Biol.*, **99**, 796-802.
Pesonen,J., Bravo,R. and Simons,K. (1984b) *J. Cell Biol.*, **99**, 803-809.
Renston,R.H., Maloney,D.G., Jones,A.L., Hradek,G.T., Wong,K.Y. and Goldfine,I.D. (1980) *Gastroenterology*, **78**, 1373-1388.
Reynolds,E.S. (1963) *J. Cell Biol.*, **17**, 208-212.
Richardson,J.C.W., Scalera,V. and Simmons,N.L. (1981) *Biochim. Biophys. Acta*, **673**, 26-36.
Rodriguez-Boulan,E. (1983) in Satir,B.H. (ed.), *Modern Cell Biology*, Vol. **1**, Alan R.Liss, NY, pp. 119-170.
Simons,K. and Fuller,S.D. (1985) *Annu. Rev. Cell Biol.*, in press.
Steinman,R.M., Brodie,S.E. and Cohn,Z.A. (1976) *J. Cell Biol.*, **68**, 665-687.
Steinman,R.M., Mellman,I.S., Muller,W.A. and Cohn,Z.A. (1983) *J. Cell Biol.*, **96**, 1-27.
Valentich,J.D. (1981) *Ann. N.Y. Acad. Sci.*, **372**, 384-405.
van Deurs,B., von Bülow,F. and Møller,M. (1981) *J. Cell Biol.*, **89**, 131-139.
Wall,D.A. and Maack,T. (1985) *Am. J. Physiol.*, **248**, C12-C20.

Received on 8 July 1985; revised on 20 August 1985

APPENDIX. Geometry of filter-grown MDCK cells

Polarity is an intrinsically quantitative phenomenon. Several aspects of cell surface polarity will be dependent on the surface areas of the two membrane domains (see Simons and Fuller, 1985). A knowledge of the geometry of the cell is, therefore, essential to an understanding of the generation and maintenance of epithelial cell polarity. This appendix describes morphometric studies of filter-grown MDCK cells.

Overview of morphometric approach

The determination of the surface areas of the plasma membrane domains of MDCK cell monolayers presents several special morphometric problems. Classically, a determination of plasma membrane surface area begins with the collection of images of randomly oriented sections of isotropically oriented cells. The length of the plasma membrane profile and the area of the cell profile would then be measured from a sufficiently large number of these images to determine the mean value of the ratio of the surface area to the volume of the cell to the desired precision. Finally, this ratio is combined with an independent, usually non-morphometric, value for the cell volume to yield the absolute cell surface area. Filter-grown MDCK monlayers are far from an ideal specimen for this approach. The monolayer is most easily sectioned perpendicular to the filter so that randomly oriented sampling cannot be assumed and would be difficult to achieve. The cuboidal cells of the monolayer are highly oriented and surface features, such as microvilli and lateral membrane infoldings, are very anisotropically distributed. Finally, no independent determination of the cell volume is available. Non-morphometric methods of volume determination, such as measuring fluid displacement following removal of cells from the filter, are prone to errors arising from non-quantitative removal of cells as well as the possibility of shape and size changes during removal. Similar considerations rule out morphometric analysis on cells which had been removed from the filter to generate an isotropic sample.

The anisotropic nature of the filter system led us to employ an anisotropic sampling procedure. We took all sections used in the analysis perpendicular to the surface of the filter. Collecting data in this way yields biased estimates of the plasma membrane domain surface area to volume ratios, but because the anisotropy in the sampling is well defined, these values can be used to calculate unbiased estimates for the parameters of interest. A further advantage of this approach is that cell parameters such as surface area and volume are obtained as functions of the boundary area of the filter. The corresponding absolute values can then be derived by using the boundary area of the filter per cell which is determined from cell counts of light micrographs taken perpendicular to the filter. This approach obviates the need for a non-morphometric measure of the cell volume. Finally, taking all sections perpendicular to the filter eases the identification of the domains of the plasma membrane, as well as allowing direct measurement of the height and the angle between the lateral membrane and the basal. Measurements of these quantities allowed us to test models for the relationship between cell size and cell shape and provided a further check on the evenness of the sampling.

Collection of morphometric data

Sections were cut perpendicular to the filter and stained with uranyl acetate and tannic acid to enhance the contrast of the plasma membrane. Representative micrographs of the sections were taken at a magnification of 3400 × following the guidelines for systematic sampling provide by Weibel (1979). Micrographs were enlarged to 10 200 × and a square grid with interline spacing equivalent to 1.49 μm was applied. The grid was aligned to an angle of 19° with the surface of the filter to give the correct mean number of intersections between the square grid and the cuboidal cell (Sitte, 1967; Eisenberg *et al.*, 1974). Intersection and point counts were performed for the frame bounded by a line drawn below the cell and parallel to the filter surface, the basal line, and the perpendiculars to it, whose intersection with the edge of the picture lay outside the cell monolayer. This procedure ensured that a known length of filter profile was beneath each sampled area. The lengths of straight lines along the basal, the lateral and the apical edges of each cell and the angles between them were also recorded. The basal membrane was defined as the plasma membrane in contact with the filter, the lateral membrane as the plasma membrane between the filter and the tight junction and the apical membrane as that above the tight junction. The number of intersections with and the number of points lying over the nuclei were also recorded.

Calculation of morphometric quantities

The calculation of morphometric values and associated statistics was performed with a pair of FORTRAN 77 programs implemented on a VAX 11/785 computer. The first program was used to enter individual image data and performed some initial consistency checks before adding it to the collection of images. The second programme was then used to select a subset of the collected images and generate the properly normalized and scaled mean values for morphometric parameters and statistics concerning them.

The area measured and the magnification varied between images. Intersection and point counts for individual images were, therefore, converted to length and

Table I. Appendix. Morphometric quantities for MDCK cells

	Strain I	Strain II
Quantities relative to filter boundary area		
Cell volume	12.90 $\mu m^3/\mu m^2$ ± 2.89%	14.14 $\mu m^3/\mu m^2$ ± 2.65%
Nuclear volume	2.21 $\mu m^3/\mu m^2$ ± 9.03%	2.46 $\mu m^3/\mu m^2$ ± 8.70%
Apical membrane area	1.85 $\mu m^2/\mu m^2$ ± 4.50%	3.05 $\mu m^2/\mu m^2$ ± 4.40%
Basal membrane area	1.47 $\mu m^2/\mu m^2$ ± 5.57%	2.18 $\mu m^2/\mu m^2$ ± 6.00%
Lateral membrane area	11.99 $\mu m^2/\mu m^2$ ± 8.25%	9.70 $\mu m^2/\mu m^2$ ± 5.30%
Total membrane	15.31 $\mu m^2/\mu m^2$ ± 6.31%	14.90 $\mu m^2/\mu m^2$ ± 3.91%
Absolute quantities		
Cell volume	1522 μm^3 ± 7.11%	1169 μm^3 ± 7.39%
Nuclear volume	261 μm^3 ± 11.10%	203 μm^3 ± 11.10%
Apical membrane area	218 μm^3 ± 7.91%	252 μm^2 ± 8.18%
Basal membrane area	172 μm^2 ± 8.65%	180 μm^2 ± 9.14%
Lateral membrane area	1404 μm^2 ± 10.50%	802 μm^2 ± 7.9%
Total membrane area	1806 μm^2 ± 9.06%	1232 μm^2 ± 7.93%
Cell count values		
Cells/filter	2.66×10^6 ± 7.00%	3.80×10^6 ± 7.50%
Cell area	118.00 μm^2 ± 6.50%	82.70 μm^2 ± 6.90%
Radius of equivalent circle	6.13 μm	5.13 μm
Electron microscopic values		
Images counted	26 pictures	22 pictures
Cells counted	90 cells	80 cells
Mean basal line length	24.7 μm ± 2.41%	25.4 μm ± 1.96%
Mean height to filter	14.2 μm ± 3.20%	15.6 μm ± 2.50%
Mean angle between lateral and base	93.7° ± 2.58%	94.3° ± 2.60%
Mean [sine (angle)]	0.950 ± 0.86%	0.955 ± 0.88%
$Sine^{-1}$ (mean [sine (angle)])	71.8°	72.7°
Mean angle between apical and base	86.1° ± 2.40%	93.7° ± 2.20%
Mean [sine (angle)]	0.964 ± 0.65%	0.962 ± 0.76%
$Sine^{-1}$ (mean [sine (angle)])	74.6°	74.2°
Mean folding factor		
Apical	1.85 ± 4.10%	3.05 ± 4.80%
Basal	1.47 ± 5.60%	2.19 ± 6.00%
Lateral	2.58 ± 3.96%	2.00 ± 5.00%
Ratios of surface areas		
Apical/basal	1.310 ± 5.21%	1.490 ± 6.83%
Basal/lateral	0.146 ± 12.40%	0.235 ± 7.28%
Apical/lateral	0.180 ± 9.16%	0.328 ± 6.34%
(Lateral + basal)/apical	7.630 ± 8.33%	4.030 ± 5.70%
Total surface area/cell volume	1.19 μm^{-1} ± 11.50%	1.05 μm^{-1} ± 10.80%

Values are expressed as the means ± the percentage standard error of the means.

area measurements and normalized by the length of the basal line to allow direct comparison of the values. Means were calculated from these normalized values after weighting with the basal line length so that the weighted mean properly reflected the area of the monolayer sampled. Thus the values for the length of the apical plasma membrane profile were calculated as:

$$(LAp)_i = \frac{(InAp)_i(MiGrd)}{(LBaLn)_i}$$

and

$$<LAp> = \sum_i^N \frac{(LAp)i(LBaLn)i}{\sum_i^N (LBaLn)i}$$

Here LAp and LBaLn represent the length, in microns, of the apical membrane profile and the basal line, respectively; MiGrd, the contour length corresponding to an intersection with the rectangular test grid. InAp, the number of intersections with the grid, < > the weighted mean value and the subscript i, which runs from 1 to N, indicating the value for an individual image. This is an extension of the procedure advocated by Cruz-Orive (1982) in which correction of individual values leads to a lower variance and hence a more efficient estimator of the morphometric quantities.

The formalism developed by Weibel (1972) and by Eisenberg *et al.* (1974) in their analyses of the highly oriented sarcomere structure formed the theoretical basis for our calculation of the unbiased estimates of surface areas and volumes. In the nomenclature of Eisenberg *et al.* (1974) the surface density of the test object per unit volume, S/V, is related to the boundary length, B, in the frame area, A, by

$$S/V = [1/k(\phi)](\bar{B}/\bar{A})$$

where

$$k(\phi) = \sqrt{\frac{1+\sin^2\phi}{2}}$$

and ϕ represents the angle which the section makes with the object. In our system the apical and basal membranes correspond to $\phi = \pi/2$ and $k(\phi) = 1/\sqrt{2}$. Thus, the ratio between the apical plasma membrane area and the basal plus lateral areas, in which the linear to areal conversion factors cancel is:

$$\frac{<LAp>}{<LBa> + \sqrt{2}<LLat>}$$

where <LAp>, <LBa> and <LLat> represent the weighted mean values of the length of the apical, basal and lateral membrane profiles, respectively. We generated absolute values of the membrane surface areas and of cell and organelle volumes by reference to the average areas of the filter occupied by a cell. This value was determined by cell counts of Hoechst-stained pieces of

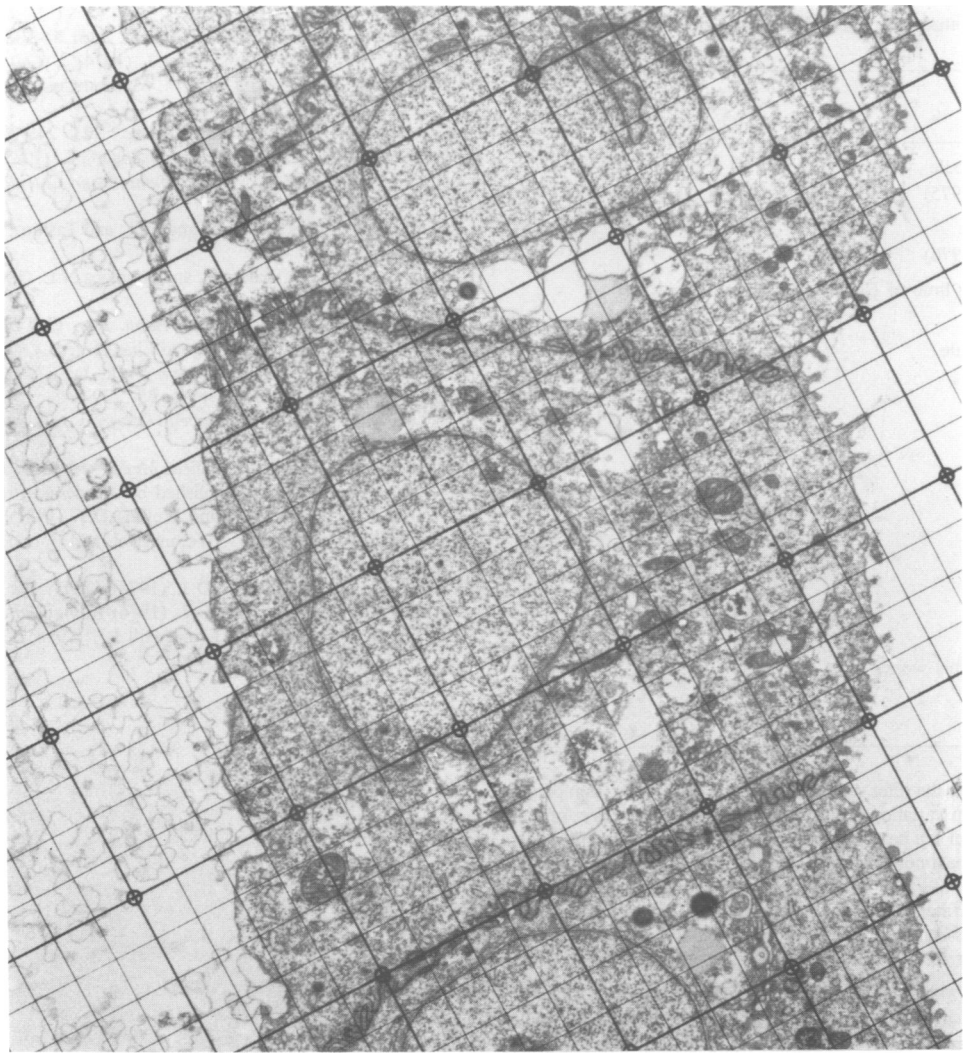

Appendix Fig. 1. Sampling grid for morphometry. Typical images of MDCK I cells used for morphometry showing the relative size of the sampling gid and of cellular features. The spacing between lines of the grid is 1.49 μm.

the same filters used for the electron microscopic morphometric measurements, following the 'forbidden line' rule (Gundersen, 1977). Quantities are expressed relative to the filter boundary following the formulation of Griffiths *et al.* (1984).

Sources of error in analysis

The results of the morphometric study of MDCK I and MDCK II cell monolayers grown on 0.45 μm filters are shown in Table I. Since the mean of the values was used for all subsequent calculations, the precision of the quantities in the table is expressed as the percentage standard error of the mean. Images were added to the data set until the standard error of the mean was $< 10\%$ for all values. The sample mean will provide a reasonable estimate of the population mean if our sample is sufficiently large to be representative and has been selected in an unbiased way. One test for bias is the comparison between the sample mean for all images and the means for subsets of the data. Four subsets of images corresponding to sections from separate blocks showed that the means lay within two standard errors of each other. Further, the standard errors of the values derived from subsets were always greater than those for the complete collection of images. The geometry of our system provides another test for how adequately our system represents the population, since the average value of the lateral edge angle must equal 90°. The observed mean angles for the samples are within 4° of this value. These considerations show that our estimates of precision are reasonable and, in particular, argue that the inclusion of more images would not significantly change the mean values which are presented in the table.

Sources of systematic error in our values must also be considered in deciding the accuracy of our results. Errors which could affect the value of one plasma membrane surface area relative to the others would be particularly damaging. The justification presented by Eisenberg *et al.* (1974) for using the 'optimal angle' method of Sitte (1967) shows that our use of a rectangular grid to sample a cuboidal structure does not favor values of one domain over the other. A bias could also arise from the mesh of the sampling grid if the features of one surface were finer than those of the others. Decreasing the mesh size of our test grid (or equivalently increasing the magnification of the image) by a factor of two did not change the surface area per filter boundary area of any of the membrane domains. This matches the impression gained from Figure 1, that the mesh size is appropriate to the features being measured. The finite thickness of the section will tend to lower the apparent value for the surface area of the membrane because grazing sections may not have sufficient contrast to be seen through the section and would be missed. This would tend to yield a lower relative value for the lateral membrane since our sections were taken perpendicular to the filter but even if an entire section width of the cell membrane was missed in this way, the underestimate would be $< 4\%$ of the actual surface area. The finer projections of the membrane could also be missed in grazing sections. This effect would be greatest for that portion of the cell parallel to the plane of section, since the projections tend to be perpendicular to the membrane and hence would lower the apparent lateral surface area by approximately the same amount as described above. This error due to grazing sections will also be mitigated by the Holmes effect (Holmes, 1927).

A major source of systematic error in our analysis would be a significant difference between the model structure of parallel cylinders perpendicular to the filter from which we derived our relationships between surface area and cell volume and the actual geometry of the cells. One obvious difference between our model and the cells is that the cell membrane is not a smooth cylinder. Weibel (1972) dealt with the case of a cylinder with a convoluted surface in his discussion of the sarcomere-associated tubule system and showed that the analysis can be extended to cylinders with convoluted surfaces by means of an area preserving mapping. A further difference from the model arises from the tilt. The cells are not

Table II. Appendix. Comparison of relative plasma membrane surface aeas of epithelial cells

	Ratio of basolateral to apical membrane area
Proximal convoluted tubule	
Welling and Welling (1975)	1.00
Proximal straight tubule	
Welling and Welling (1976)	1.01
Cortical thick ascending limb of Henle	
Welling *et al.* (1978)	9.68
Cortical connecting tubule (Welling *et al.*, 1981)	
Principal cell	17.98
Intercalated cell	5.96
Cortical collecting duct (Welling *et al.*, 1983)	
Principal cell	12.05
Intercalated cell	5.63
Hepatocyte	
Weibel (1976)	6.77
Matsuura *et al.* (1982)	6.24
MDCK cell on filters (this work)	
Strain I	7.63
Strain II	4.03

all strictly perpendicular to the filter surface and further departures from perpendicularity will result from variation in the angle of section. The effect of these departures from the model can be evaluated from the expression for $k(\phi)$ shown above. We estimate our maximum error in sectioning angle to be 5° which would result in a change in $k(\phi)$ of $<0.75\%$. Similarly, the average value of the sine of the angle between the filter and the lateral edge is >0.95 which would yield an error in $k(\phi)$ of $<2.5\%$. In summary, these systematic errors are smaller than the precision of our mean values.

Morphology of MDCK cells

The values in Table I reveal that filter-grown MDCK cells resemble a cuboidal epithelium; the diameter of the cell is only slightly less than its height. The degree of folding of the plasma membrane is represented numerically as the folding factor, the ratio of the actual length of the plasma membrane profile to a straight line along it. The folding factors for all the domains of the cell are greater than one showing that the plasma membrane is highly convoluted. The availability of firm values for the geometry of the cell allows a definitive comparison of the morphologies of the two strains of MDCK. Strain II cells are taller, narrower and have a slightly smaller volume than strain I cells grown under identical conditions. The ratios of the plasma membrane area to cell volume are equal for the two strains within experimental error and similar to those reported for L cells (1.16/μm) and BHK cells (0.89/μm). A marked difference between the two strains is seen in the folding factors of the lateral and apical membranes. In strain I cells, the lateral membrane is the most heavily folded of the three domains with the apical and basal membranes showing similar degrees of folding. The situation is reversed in strain II cells where the apical membrane is much more folded than the lateral, which displays a similar degree of folding to the basal. The weighted mean folding factors for the two strains are similar (2.15 for strain I versus 2.24 for strain II) so that a general increase in membrane folding is not the cause of this difference.

Comparison of the results of morphometry on the rabbit renal epithelia (Table II) helps to place our MDCK results in perspective. As one moves from the proximal tubule to the collecting duct two general trends are seen. The lateral surface becomes increasingly convoluted while the apical surface becomes smoother. The result of these two trends is that the apical surface becomes a smaller fraction of the total cell surface changing from $\sim 50\%$ to $\sim 5.6\%$. Our MDCK results are consistent with the cells being derived from the more distal portion of the nephron. This matches several other properties of these cells which they also have in common with collecting duct and distal tubule cells (Richardson *et al.*, 1981; Herzlinger *et al.*, 1982). This observation of greater basolateral surface area than apical has also been made in the work of Weibel (1976) and of Matsuura *et al.* (1982) on the hepatocyte.

References

Cruz-Orive,L.-M. (1982) *J. Microsc.*, **125**, 84-102.

Eisenberg,B., Kuda,A. and Peter,J. (1974) *J. Cell Biol.*, **60**, 732-754.

Griffiths,G., Warren,G., Quinn,P., Mathieu-Costello,O. and Hoppeler,H. (1984) *J. Cell Biol.*, **98**, 2133-2141.

Gundersen,H.-J.G. (1977) *J. Microsc.*, **111**, 219-223.

Herzlinger,D.A., Easton,T.G. and Ojakian,G.K. (1982) *J. Cell Biol.*, **93**, 269-277.

Holmes,A. (1927) *Petrographic Methods and Calculation*, published by Murby, London.

Matsuura,S., Nakada,H., Sawamura,T. and Tashiro,Y. (1982) *J. Cell Biol.*, **95**, 864-875.

Richardson,J.C.W., Scalera,V. and Simmons,N.L. (1981) *Biochim. Biophys. Acta*, **673**, 26-36.

Simons,K. and Fuller,S. (1985) *Annu. Rev. Cell Biol.*, in press.

Sitte,H. (1967) in Weibel,E.R. and Elias,H. (eds.), *Quantitative Methods in Morphology*, Springer-Verlag, New York, Inc., NY, p.167.

Weibel,E.R. (1972) *J. Microsc.*, **95**, 229-242.

Weibel,E.R. (1976) *Sixth European Congress on Electron Microscopy*, Jerusalem; pp. 6-9.

Weibel,E.R. (1979) *Stereological Methods. Vol. 1. Practical Methods for Biological Morphometry*, published by Academic Press, London.

Welling,L.W., Evan,A.P. and Welling,D.J. (1981) *Kidney Int.*, **20**, 211-222.

Welling,L.W., Evan,A.P., Welling,D.J. and Gattone,V.H. (1983) *Kidney Int.*, **23**, 358-367.

Welling,L.W. and Welling,D.J. (1975) *Kidney Int.*, **8**, 343-348.

Welling,L.W. and Welling,D.J. (1976) *Kidney Int.*, **9**, 385-394.

Welling,L.W., Welling,D.J. and Hill,J.J. (1978) *Kidney Int.*, **13**, 144-151.